Traffic


Published by John Wiley & Sons Ltd
doi:10.1111/tra.12209

Toolbox

# Targeting of Viral Capsids to Nuclear Pores in a Cell-Free Reconstitution System

**Fenja Anderson[1†], Anca F. Savulescu[2†‡], Kathrin Rudolph[1], Julia Schipke[1], Ilana Cohen[3], Iosune Ibiricu[4§], Asaf Rotem[3¶], Kay Grünewald[4], Beate Sodeik[1*†] and Amnon Harel[2*†]**

[1]Institute of Virology, OE 5230, Hannover Medical School, Carl-Neuberg-Straße 1, D-30623 Hannover, Germany
[2]Faculty of Medicine in the Galilee, Bar-Ilan University, 8 Henrietta Szold Street, Safed 1311502, Israel
[3]Department of Biology, Technion – Israel Institute of Technology, Haifa 32000, Israel
[4]Oxford Particle Imaging Centre, Division of Structural Biology, Welcome Trust Centre for Human Genetics, University of Oxford, Oxford, UK

*Corresponding authors: Beate Sodeik, sodeik.beate@mh-hannover.de and Amnon Harel, amnon.harel@biu.ac.il

## Abstract

Many viruses deliver their genomes into the nucleoplasm for viral transcription and replication. Here, we describe a novel cell-free system to elucidate specific interactions between viruses and nuclear pore complexes (NPCs). Nuclei reconstituted *in vitro* from egg extracts of *Xenopus laevis*, an established biochemical system to decipher nuclear functions, were incubated with GFP-tagged capsids of herpes simplex virus, an alphaherpesvirus replicating in the nucleus. Capsid binding to NPCs was analyzed using fluorescence and field emission scanning electron microscopy. Tegument-free capsids or viral capsids exposing inner tegument proteins on their surface bound to nuclei, while capsids inactivated by a high-salt treatment or covered by inner and outer tegument showed less binding. There was little binding of the four different capsid types to nuclei lacking functional NPCs. This novel approach provides a powerful system to elucidate the molecular mechanisms that enable viral structures to engage with NPCs. Furthermore, this assay could be expanded to identify molecular cues triggering viral genome uncoating and nuclear import of viral genomes.

**Keywords** herpes simplex virus, herpesviruses, nuclear pore, reconstitution, *Xenopus* nuclei

Received 27 March 2014, revised and accepted for publication 13 August 2014, uncorrected manuscript published online 18 August 2014, published online 12 September 2014

More than 30 proteins termed nucleoporins (Nups) assemble into nuclear pore complexes (NPCs) that serve as specialized gateways in the nuclear envelope to allow active and passive bidirectional molecular traffic between the cytosol and the nucleoplasm (1–3). The structural organization of NPCs is similar in humans and amphibians; both possess a central channel with an inner diameter of about 50 nm at their center surrounded by an elaborate scaffold structure with eightfold rotational symmetry (4,5). Their nucleoplasmic face is capped by the nuclear basket, while filaments of up to 50 nm in length protrude freely from the cytosolic face. NPCs allow the passage of molecules up to about 5 nm in diameter by diffusion, while shuttling nuclear transport receptors, called importins and exportins, are required for active translocation of cargoes (6–8). A RanGTP/RanGDP gradient across the nuclear envelope and members of the importin β superfamily control the directionality of transport, but the translocation process itself does not require GTP hydrolysis (8–12).

[†]These authors contributed equally.
[‡]Present address: Synthetic Biology – ERA, CSIR Biosciences, Pretoria, South Africa.
[§]Present address: Department of Pathology, CDIPD, Universidad de California, San Francisco, CA, USA.
[¶]Present address: Biological Chemistry & Molecular Pharmacology, Harvard Medical School, Boston, MA, USA.

Herpesviruses comprise a large group of DNA viruses that have been identified from humans to mollusks (13). Herpes simplex virus type 1 (HSV1) is a human alphaherpesvirus with a genome of 152 kb that is packaged into an icosahedral capsid of 125 nm in diameter (14). The major capsid protein VP5 forms 150 hexons on the capsid faces and edges and 11 pentons at the vertices, while the 12th vertex is occupied by a dodecamer of pUL6 that operates as a portal (15). The capsids are enclosed by an eccentric tegument of about 25 distinct proteins that have been classified into a more ordered inner and a less structured outer layer (16–22). The outer tegument binds to cytosolic domains of viral glycoproteins embedded into the viral envelope, overall forming a virion of about 225 nm in diameter (16,22). Three types of capsids can be readily purified from the nuclei of infected cells (cf. Figure 1, top left): C capsids, which are the heaviest on sedimentation gradients, contain viral genomes; B capsids contain the scaffold proteins but no DNA; and A capsids, which are empty, lack both scaffold proteins and DNA. The packaging of progeny genomes into nuclear rather spherical pro-capsids results in the formation of C capsids that are then predominantly exported across the nuclear envelope, while the nuclear A and B capsids are considered dead-end products (14,23). The cytosolic capsids recruit inner tegument proteins such as pUL36 and pUL37 and are transported to cytoplasmic membranes to acquire the outer tegument and their envelopes (22–26). The virions are transported within secretory vesicles to the plasma membrane for release by exocytosis (22–24).

After HSV1 cell entry by fusion with host membranes, inner tegument proteins such as pUL36 and pUL37 remain capsid-associated, while most or all outer tegument proteins detach (25–31). The capsids recruit the motor protein dynein and its cofactor dynactin for transport along microtubules toward the nucleus (32,33). Electron microscopy images show parental capsids interacting with the cytosolic filaments emanating from NPCs, with one vertex facing the central channel (33–39). While most of these capsids appear empty, fortuitous cross sections seem to visualize the viral DNA genome as it is ejected from one vertex through the NPC (33,39). Similarly, after a short adsorption to a solid surface, the DNA is also ejected *in vitro* as a single double helix from one vertex, most likely the portal (40). These observations are consistent with the notion that HSV1 utilizes energy from ATP hydrolysis to pack genomes into capsids, while a pressure-driven mechanism pushes the genomes out of the capsids and through the permeability barrier of NPCs (41–43). The capsids are able to withstand this internal pressure by further stabilization of the capsid shell that seems to be initiated by DNA packaging after protein scaffold expulsion (44).

A biochemical cell-free system based on *Xenopus laevis* extracts has greatly aided studies of NPC assembly and nuclear transport (cf. Figure 1, right). Adding chromatin to fractionated egg extracts triggers a complex series of events including membrane vesicle recruitment, vesicle fusion and assembly of NPCs into the newly forming nuclear envelopes (45–48). NPC assembly can be blocked by the addition of Imp $\beta^{45-462}$, a truncated form of importin β, or by the $Ca^{2+}$-chelator BAPTA [1,2-bis(*o*-aminophenoxy)-ethane-*N*,*N*,*N*′,*N*′-tetraacetic acid], resulting in the formation of apparently pore-free nuclei in which the chromatin is fully enclosed by membranes lacking any signs of NPCs (49). These and other biochemical interventions make this *in vitro* system a powerful tool for the analysis of various nuclear functions (50).

Much remains to be learned about capsid docking at NPCs, viral genome uncoating, and viral genome translocation into the nucleoplasm. As NPCs are essential for cell survival, it is a challenge to elucidate their function in intact cells. Our first *in vitro* study has shown that isolated HSV1 capsids derived from extracellular virions by Triton-X-100 (TX-100) lysis in the presence of 0.5 M NaCl can bind to nuclei isolated from rat liver, and that importin β, the RanGTP/GDP cycle and capsid-NPC interactions are required to trigger the release of the viral genomes (37). Similarly, capsids isolated from virions by TX-100 lysis in the presence of 0.5 M KCl interact *in vitro* with dynein, its cofactor dynactin, kinesin-1 and kinesin-2 from both pig brain cytosolic extracts and *Xenopus* egg extracts, and assemble functional capsid–motor complexes that can translocate along microtubules *in vitro* [summarized in Table 1; (19,20,51)].

These studies show that key virus–host interactions are conserved from amphibians to mammals, and that capsids derived from extracellular virions by detergent lysis at 0.5 M NaCl or 0.5 M KCl maintain their affinity for specific host factors. By contrast, capsids isolated from the nuclei of infected cells, or capsids prepared by detergent

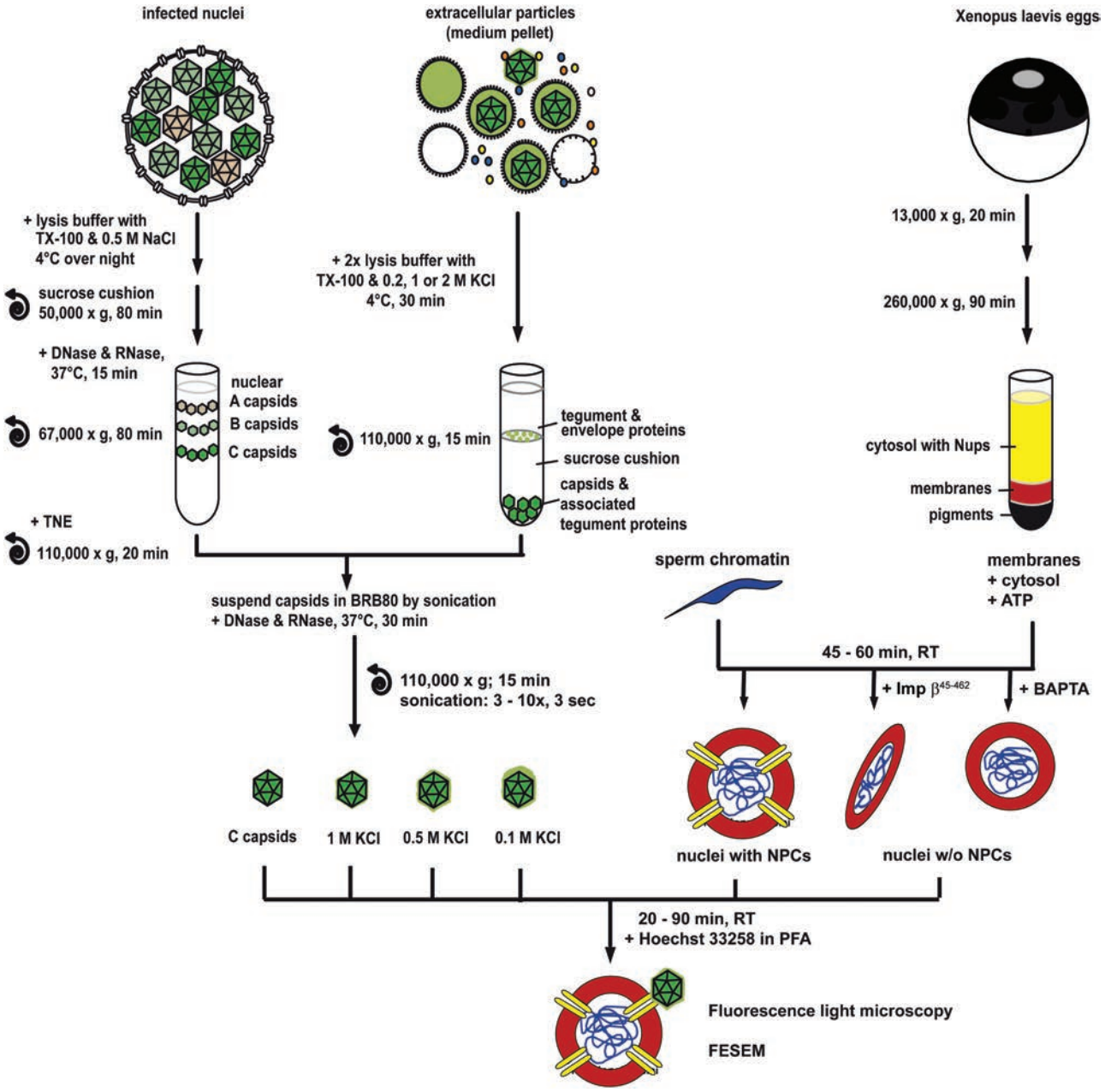


**Figure 1: An *in vitro* assay to analyze the binding of viral capsids to NPCs**. Nuclear capsids (dark green) were isolated from the nuclei of HSV1-infected cells by gradient sedimentation (top left). Viral capsids were generated from mature extracellular particles released from HSV1-infected cells by lysis with 1% TX-100 in the presence of 1, 0.5 or 0.1 KCl (light and dark green) and purified through sucrose cushions (top middle). The four different capsid types were re-suspended in BRB80 buffer before tip sonication and DNase/RNase treatment. Nuclei harboring functional NPCs were generated *in vitro* from *Xenopus* egg extracts around a chromatin template. The formation of NPCs was inhibited in some reactions by the addition of Imp $\beta^{45-462}$ or BAPTA to the assembly reaction to create nuclei enclosed by continuous membranes lacking functional NPCs (top right). After nuclear assembly and re-sedimentation, the nuclear or viral 1, 0.5 or 0.1 M capsids were incubated with different nuclei for 20–90 min at room temperature. Nuclear assembly and capsid binding were analyzed by fluorescence light microscopy or field emission scanning electron microscopy (FESEM). Modified from figure 1 of (19).

**Table 1:** Protein characterization of isolated HSV1 capsids

| Association of host factors | Detection method | Viral (0.5 M KCl) | Nuclear (IB on B and C, IEM on B and C) | Viral (1 M KCl) | Viral (0.1 M KCl) |
|---|---|---|---|---|---|
| Dynein | IB | +++ | – | +++ | – |
| | IEM (%) | 100 | 0 | 98 | 33 |
| Dynactin | IB | +++ | – | ++ | – |
| | IEM(%) | 100 | 0 | 66 | 3 |
| Kinesin-1 | IB | +++ | – | – | – |
| | IEM (%) | 100 | 0 | 19 | 4 |
| Kinesin-2 | IB | +++ | – | ++ | + |
| | IEM (%) | 100 | 35 | 43 | 0 |
| **HSV1 proteins (copies/virion)** | | | | | |
| *Capsid proteins* | | +++ | +++ | +++ | +++ |
| VP5 (955) | MS (mass spectrometry) (%) | 100 | 100 | 100 | 100 |
| VP19c (320) | MS (%) | 100 | 100 | 100 | 100 |
| VP23 (640) | MS (%) | 100 | 100 | 100 | 100 |
| VP24 (150) | MS (%) | 100 | 100 | 100 | 100 |
| VP26 (600) | MS (%) | 100 | 100 | 100 | 100 |
| pUL17 (60) | IB | +++ | +++ | +++ | +++ |
| | MS (%) | 100 | 100 | 100 | 100 |
| pUL25 (60) | IB | +++ | +++ | +++ | +++ |
| | MS (%) | +++ | +++ | +++ | +++ |
| | IEM (%) | ++ | ++ | +++ | ++ |
| *Inner tegument proteins* | | +++ | – | +++/– | +++ |
| pUS3 (?) | IB | +++ | + | +++ | +++ |
| | IEM (%) | 90 | 19 | 75 | 100 |
| pUL36 (150) | IB middle | ++ | –/+ | ++ | +++ |
| | MS (%) | 28 | – | 18 | 20 |
| | MS – Nterm (%) | 189 | – | 183 | 161 |
| | IEM – middle Ab (%) | 100 | 1 | 81 | 76 |
| | IEM – Cterm Ab (%) | 100 | 36 | 2 | 58 |
| pUL37 (150) | MS (%) | 49 | – | 21 | 48 |
| | IEM (GFP) (%) | 94 | 1 | 32 | 100 |
| ICP0 (?) | IB | +++ | – | ++ | +++ |
| pUL14 (?) | IB | +++ | + | +++ | +++ |
| pUL16 (?) | MS (%) | 45 | – | 21 | 42 |
| pUL21 (?) | MS (%) | 55 | – | 19 | 50 |
| *Outer tegument proteins* | | ++ | – | + | +++ |
| pUL41 – vhs (?) | IB | ++ | – | + | +++ |
| pUL11 (?) | IB | + | – | + | +++ |
| ICP4 (?) | IB | ++ | – | + | +++ |
| ICP34.5 (?) | IB | ++ | – | ++ | +++ |
| VP13/14 (1300–1800) | MS (%) | 65 | – | 12 | 124 |
| | IEM (%) | 71 | –/+ | 56 | 100 |
| VP16 (700–2000) | MS (%) | 41 | – | 19 | 72 |
| | IEM (%) | 89 | –/+ | 65 | 100 |
| VP22 (700–1500) | MS (%) | 55 | – | 23 | 143 |
| | IEM (%) | 72 | –/+ | 24 | 100 |

IB, immunoblot; IEM, immunoelectron microscopy; MS, mass spectrometry.

HSV1 capsids were isolated from extracellular virions using TX-100 in the presence of 0.1, 0.5 or 1 M KCl or from infected nuclei (nuclear), and the association of microtubule-associated factors was analyzed by immunoblot and quantitative electron microscopy (19). Furthermore, the composition of structural HSV1 proteins was analyzed by immunoblot, quantitative mass spectrometry and quantitative immunoelectron microscopy (summarized in 51). The signal intensities of the immunoblots for each protein were evaluated qualitatively (+++ for the strongest band, ++, +, and – if there was no or only a negligible band) (19). For mass spectrometry data, the amount of the respective protein in gradient-purified extracellular virions was set to 100%, and the amount of the proteins present on the respective viral capsids were normalized accordingly (19). For the immunoelectron microscopy, the labeling intensity of the capsid type with the highest amount of surface labeling was set to 100%, and the labeling intensities on the other capsids were normalized accordingly. The information on the estimated copy number per virion (copies/virion) was compiled from several reports (17,21,68,87–89). The ? in brackets indicates that the copy number/virion is not known for this structural HSV1 protein.

lysis of extracellular virions in the presence of 0.1 M KCl do not bind to microtubule motors, while viral capsids isolated in the presence of 1 M KCl maintain their ability to interact with dynein, but no longer bind to kinesins [summarized in Table 1; cf. Figure 1 left; (19,20)]. Our subsequent immunoblot analysis, quantitative mass spectrometry and quantitative immunoelectron microscopy studies have shown that viral capsids treated with 0.5 M KCl expose the inner tegument proteins pUL36, pUL37 and pUS3 and only low amounts of outer tegument proteins such as VP13/14, VP16 and VP22, while capsids treated with 0.1 M KCl harbor, in addition to inner tegument, high amounts of outer tegument [summarized in Table 1; (19,20)].

In this report, we describe a novel cell-free assay that measures the binding of HSV1 capsids to reconstituted *Xenopus* nuclei (cf. Figure 1, bottom). Our results show that nuclear capsids that display only outer capsid proteins on their surfaces and 0.5 M KCl viral capsids exposing outer capsid proteins in addition to inner tegument proteins, but not the other viral capsid types, bind specifically to nuclei harboring functional NPCs. This new biochemical assay has broad potential for the study of interactions between viral structures with distinct components of the NPC as well as the nuclear import of viral proteins and genomes for transcription and replication.

## Results

### HSV1 capsids with defined surface features

To identify the role of HSV1 structures in binding to NPCs, we prepared capsids characterized by different surface features. To isolate nuclear capsids (cf. Figure 1, left), we treated infected cells prior to lysis with two different buffers: with TNE (Tris-NaCl-EDTA buffer) containing 0.5 M NaCl as reported by Newcomb and Brown (52,53), or with MKT (MES-KCl-Tris buffer) containing a physiological concentration of 0.1 M KCl before cell lysis as described in our previous studies (19,20,51). Viral capsids were prepared from extracellular virions using TX-100 in the presence of 1, 0.5 or 0.1 M KCl as described in our previous studies (19,20); cf. Figure 1, middle). Immunoblot analysis did not reveal any differences in the protein composition of the different nuclear capsid preparations irrespective of the buffer used prior to cell lysis (Figure 2). Nuclear capsids contained the capsid proteins VP5, VP19c and VP23 in similar amounts to viral capsids, although there were some minor variations between different preparations. B capsids also contained the scaffold proteins VP21 and VP22a. The amount of pUL25 was similar on A, B and C capsids, but appeared higher on viral capsids than on nuclear capsids. When compared with such nuclear capsids, the three types of viral capsids also contained similar amounts of the inner tegument proteins pUL36 and pUL37. By contrast, the outer tegument protein VP13/14 was most prominent on viral 0.1 M KCl capsids, but not present on nuclear capsids, consistent with our previous analysis [summarized in Table 1; (19,20,51)].

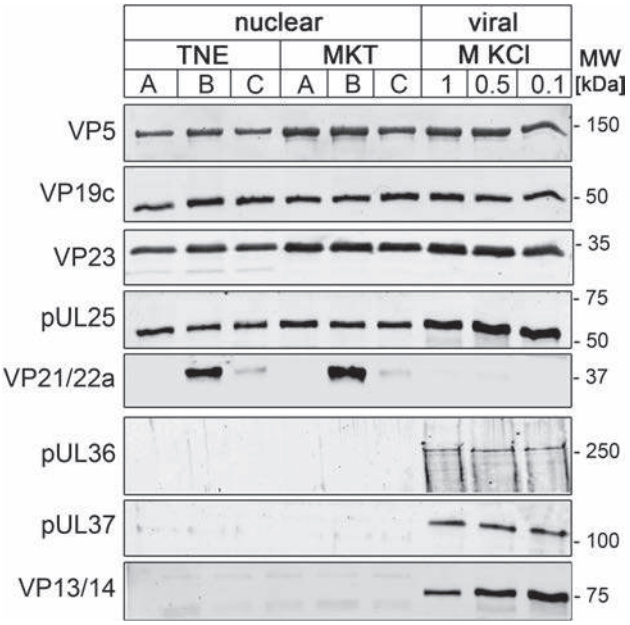


**Figure 2: Protein composition of different HSV1 capsids types**. Nuclear capsids were isolated from BHK cells infected with HSV1-GFPVP26 using TNE or MKT buffer for cell suspension, and their protein composition was compared with that of viral capsids treated with TX-100 and 1.0, 0.5 or 0.1 M KCl by immunoblotting with antibodies raised against the capsid proteins VP5 (mAb H1.4), pUL25 (mAb #166), VP19c (pAb NC2), VP21/VP22a (pAb NC3/4) or VP23 (pAb NC5), or the tegument proteins pUL36 (pAb #147), pUL37 (pAb anti-pUL37) or VP13/14 (pAb R220).

We next analyzed the capsid surfaces using electron cryo tomography and sub-volume averaging, and compared the degree of tegumentation of viral capsids to that of nuclear C capsids (Figure 3). As viral capsids had a tendency to aggregate, we selected single capsids present in the holes of

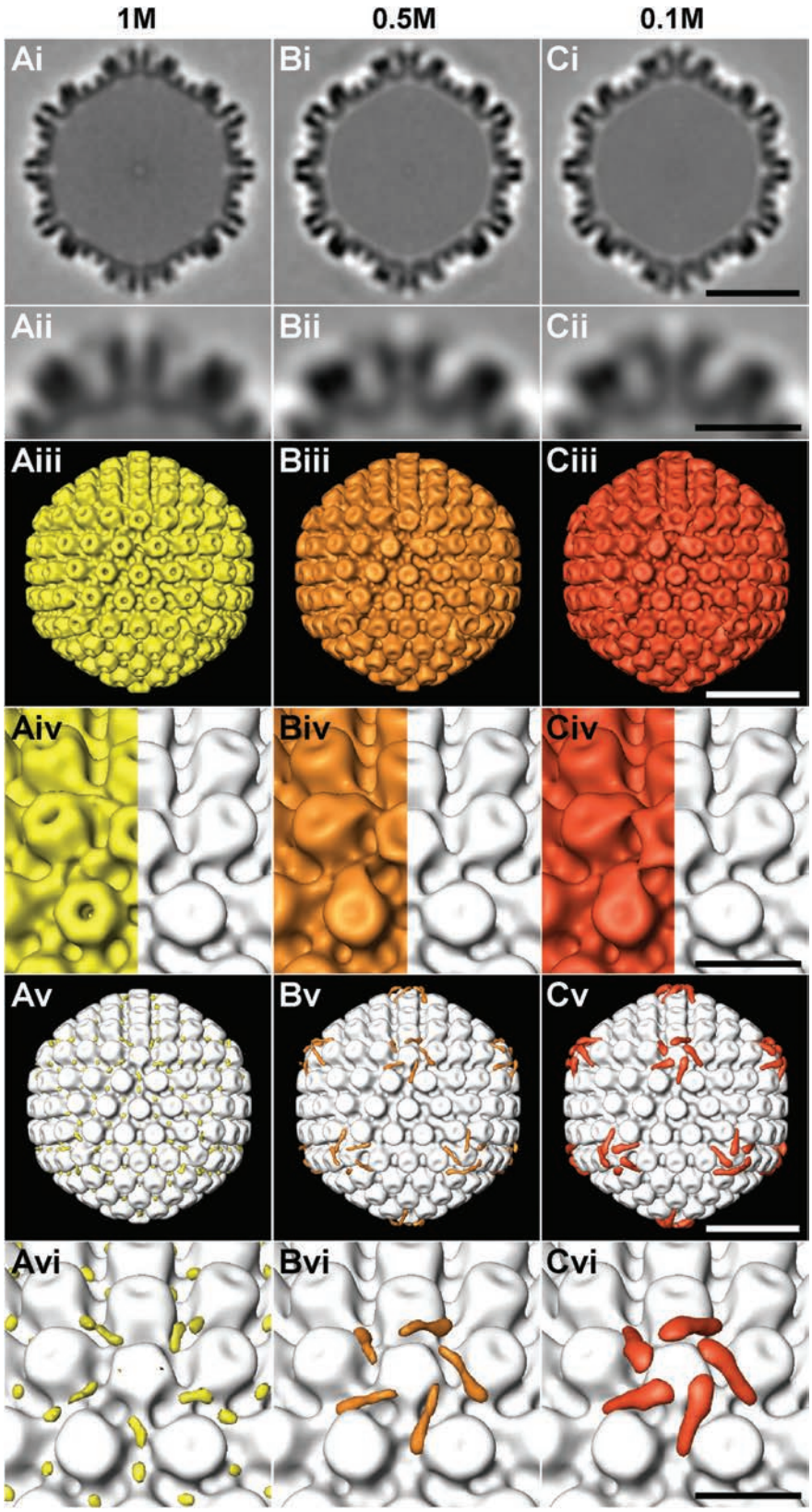


**Figure 3: Electron cryo tomography reveals surface features of different HSV1 capsid types**. Results from sub-volume averaging are presented for capsids isolated from intact virions (HSV1 strain F) and extracted with TX-100 and 1 M (A), 0.5 M (B) or 0.1 M (C) KCl. Row (i): cross sections of the averages from 183 (1 M), 246 (0.5 M) or 217 (0.1 M) capsid sub-volumes. Scale bar: 50 nm. Row (ii): close-up view of the top vertex in row (i). Scale bar: 20 nm. Row (iii): iso-surface representation of the averages. Scale bar: 50 nm. Row (iv): close-up view of a salt-treated capsid vertex (left), compared to nuclear C capsids (66). Scale bar: 20 nm. Row (v): difference map between the respective salt-treated capsid group and the nuclear C capsids average, superimposed onto the nuclear C capsids average. Scale bar: 50 nm. Row (vi): close-up view of a vertex from row. Scale bar: 20 nm. (v). The capsids have a diameter of 125 nm.

the carbon support film for analysis. In total, we averaged 183, 246 or 198 capsids isolated in the presence of 1, 0.5 or 0.1 M KCl, respectively. The capsid averages were filtered to a resolution of 5.6 nm, and the differences in densities were calculated by subtracting the gray values of nuclear capsids from those of KCl-treated capsids. We detected little differences between viral capsids treated with 1 M KCl and nuclear capsids (yellow in Figure 3Av,vi). By contrast, there was a clear extra density on viral capsids prepared with 0.5 M KCl (orange in Figure 3Bv,vi) and even more pronounced on 0.1 M KCl capsids (red in Figure 3Cv,vi). These densities were located at the vertices protruding from the top of the pentons and from one side of the neighboring hexons, but not on the other hexons. Thus, viral and nuclear HSV1 capsids vary substantially in their protein composition and in their surface structure, and may therefore differ in their interactions with shuttling nuclear transport receptors and NPCs.

### Nuclei harboring NPCs reconstituted from *Xenopus laevis* egg extracts

To develop a novel method to study capsid interactions with NPCs, we assembled nuclei *in vitro* from *X. laevis* egg extracts. De-membranated sperm chromatin was incubated with membrane vesicles as a source for nuclear membranes and a cytosolic fraction as a source for Nups [Figure 1, top left; (46,54)]. Nuclear assembly was validated for each experiment by labeling with the monoclonal antibody mAb414 recognizing FG-repeat Nups in mature NPCs (55). A rim-like signal around the chromatin indicated the formation of nuclei surrounded by nuclear envelopes harboring NPCs (Figure 4Aii). No NPC staining was observed when either Imp $\beta^{45-462}$ (Figure 4Bii) or BAPTA (Figure 4Cii) had been added to the reconstitution mixture. Furthermore, TRITC-NLS-BSA, a reporter cargo of the classical importin α/β pathway, was imported into functional control nuclei (Figure 4Aiv), but not into pore-free nuclei (Figure 4Biv,Civ).

### An *in vitro* assay to decipher the interactions of viral capsids with NPCs

To detect capsids, we used an HSV1-GFPVP26 strain in which the outer capsid protein VP26 has been replaced by a GFPVP26 fusion protein that is incorporated into virions during capsid assembly (56). Although a fraction of GFPVP26 seems to dissociate during cytosolic passage in epithelial cells, sufficient amounts remain associated with and are detected on HSV1 capsids docked at the nuclei (57). Furthermore, HSV1-GFPVP26 capsids utilize microtubule transport and, like wild-type capsids, recruit dynein from cytosolic extracts of *X. laevis* eggs (20,57). Thus, the GFP tag on VP26 does not interfere with crucial cytosolic capsid–host interactions. Of the capsids tested here, viral capsids treated with 0.5 M KCl are most similar in terms of protein composition to the ones that bind to NPCs of rat liver nuclei or to microtubule motors (19,20,37). To investigate whether such capsids can also bind to *Xenopus* NPCs, we incubated 0.5 M KCl viral capsids of HSV1-GFPVP26 with reconstituted nuclei. To delineate the nuclear envelopes, fluorescent Imp $\beta^{45-462}$ was added during the last 10 min of the respective binding reaction. Initial time course experiments revealed that the number of bound capsids varied between the different capsid types and preparations, but remained rather constant during a time window of 30–90 min (data not shown). While surface views in top and bottom confocal laser microscopy sections showed punctate labeling typical of NPCs (Figure 4Di, red in 4Diii) and HSV1 capsids scattered over the nuclear surface (Figure 4Dii, green in Diii), midsections revealed capsids (Figure 4Eii, green in Eiii, white arrowheads) closely juxtaposed to the rim labeling of the nuclear envelopes (Figure 4Ei, red in Eiii).

To obtain further information on the association of capsids with *Xenopus* nuclei, we used high-resolution field emission scanning electron microscopy (FESEM) to image the nuclear surface. Samples were labeled with a polyclonal antiserum raised against viral capsids, followed by anti-rabbit-antibodies conjugated to 12 nm colloidal gold particles. The three-dimensional surface topography of reconstituted nuclei, including the cytoplasmic surface of NPCs, is seen in the in-lens images (Figure 4F), while the corresponding backscatter electron detector images reveal the position of gold-conjugated antibodies (Figure 4G). Thus, HSV1 capsids could be unequivocally identified by multiple gold particles, which often lined up along the capsid edges and vertices (Figure 4G; white arrowheads). Each capsid blocked a considerable area of the nuclear envelope from view, but depending on the imaging angle, it was possible to obtain partial views of NPCs underneath the capsids (Figure 4Fi,ii; white arrows). Controls in which either the capsids or the primary antibodies had been

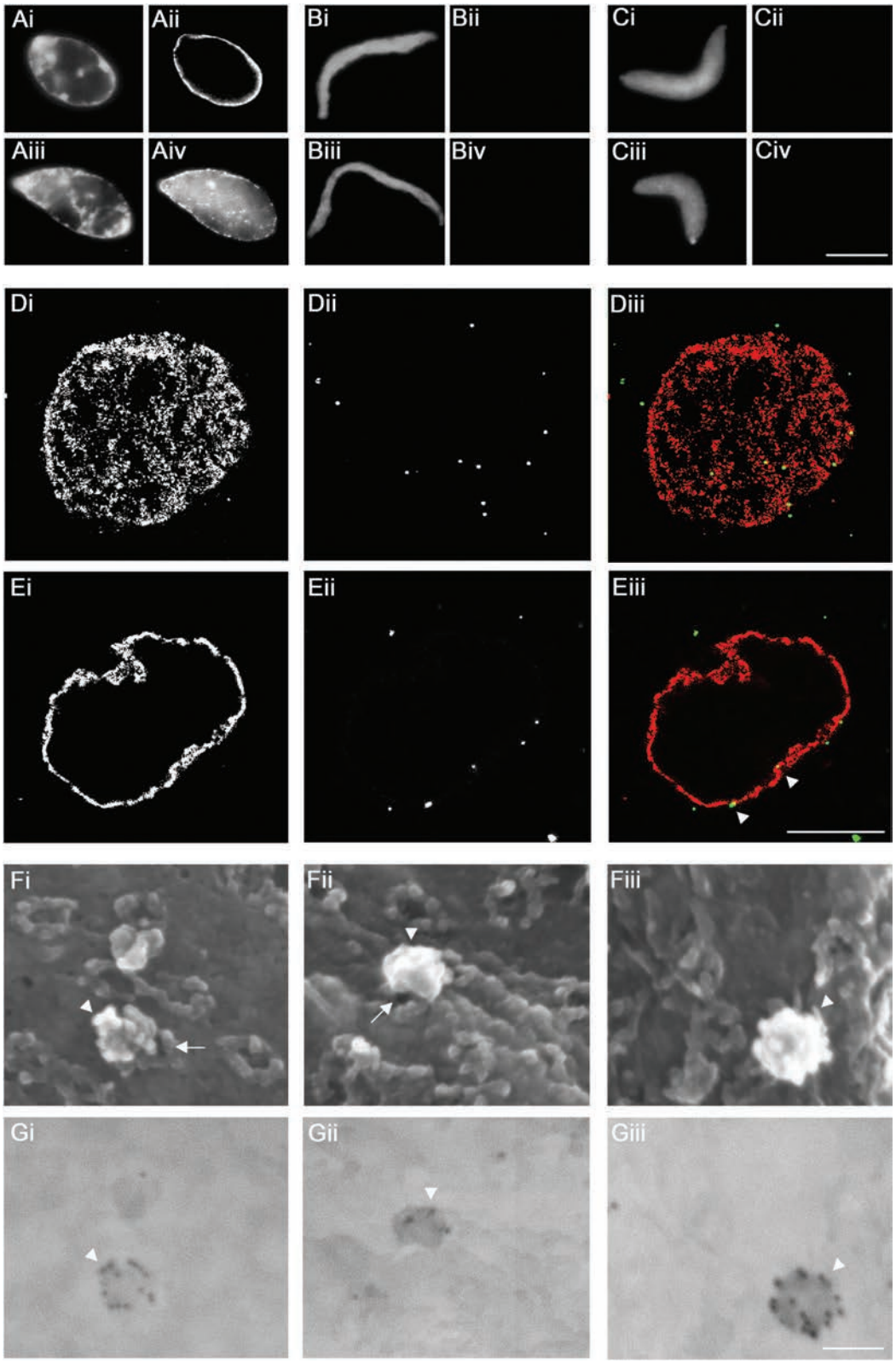


**Figure 4:** Legend on next page.

omitted revealed little background labeling (not shown). These experiments demonstrated that HSV1 capsids are capable of docking onto NPCs of *in vitro* reconstituted *Xenopus* nuclei.

### Specific capsid features and functional NPCs are required for HSV1 capsid binding to *Xenopus* nuclei

To determine which HSV1 capsid types were targeted to NPCs, we tested nuclear C capsids, as well as viral capsids extracted at 1, 0.5 or 0.1 M KCl, for binding to functional nuclei harboring NPCs or to pore-free nuclei assembled in the presence of Imp $\beta^{45-462}$ or BAPTA. Several images of HSV1-GFPVP26 capsids were acquired by epi-fluorescence microscopy at different focal planes, merged and superimposed with a middle focal plane image of the DNA-stained nucleus. Only immobile capsids colocalizing with the DNA were scored as bound to nuclei, and their number was determined for 5–20 nuclei in each condition. This setup allowed a comparison of several conditions on the same day. However, no binding of HSV1 capsids to *Xenopus* nuclei was observed if either component had been stored for several hours at room temperature, on ice or frozen. Instead, it was mandatory to isolate HSV1 capsids for each experiment and to reconstitute *Xenopus* nuclei just prior to their co-incubation, and only a few parameters could be compared within one given experiment. Therefore, we integrated all experiments into one analysis, although some conditions had been evaluated more often than others (Table 2).

To summarize the data of many experiments in a comparative manner, we set the mean number of the 0.5 M KCl viral capsids (14.8 capsids) bound per functional nucleus to 100% (Table 2, Figure 5). All types of viral and nuclear C capsids were targeted to *Xenopus* nuclei to some extent, with the viral 0.5 M KCl capsids and the nuclear capsids showing the highest degree of binding. While the number of viral 0.5 M KCl capsids was comparable to that of nuclear capsids, 0.1 and 1 M capsids bound significantly less efficiently ($p = 0.001$). Furthermore, the binding of all capsid types was substantially reduced for nuclei that had been reconstituted in the presence of Imp $\beta^{45-462}$ or BAPTA. As the binding of 1 M viral capsids to BAPTA-treated nuclei was the lowest of all conditions tested, it may be considered as nonspecific background. These results show that HSV1 capsids docked specifically onto NPCs of *in vitro* reconstituted *Xenopus* nuclei, and that this interaction was mediated by outer capsid and/or inner tegument proteins exposed in a functional conformation on the surface of 0.5 M KCl and nuclear C capsids.

## Discussion

### A cell-free assay to analyze viral interactions with NPCs

Very few biochemical studies have been able to address an association of viral structures with NPCs (37,58–61). To study the nuclear targeting of mammalian viruses, we have harnessed *Xenopus* nuclei reconstituted *in vitro* that have been used extensively to study nuclear assembly and nuclear transport (48,54,62,63). HSV1 viral capsids, isolated from virions with TX-100 in the presence of 0.5 M KCl, as well as nuclear C capsids interacted specifically with nuclei harboring functional NPCs. High-resolution

**Figure 4: Targeting of HSV1 capsids to NPCs on *Xenopus* nuclei *in vitro*.** A–C). Functional (A), Imp $\beta^{45-462}$ (B) or BAPTA (C) nuclei were reconstituted *in vitro*. Completion of nuclear assembly was monitored by epi-fluorescence microscopy by DNA staining with Hoechst 33258 (i and iii), NPC staining with fluorescently labeled mAb414 (ii) and the transport capacity of the assembled NPCs was confirmed by the nuclear import of TRITC-NLS-BSA (iv). Scale bar: 10 μm. D,E) Binding of viral 0.5 M KCl capsids extracted from extracellular particles of HSV1-GFPVP26 (ii and iii, green, white arrowheads) to *Xenopus* nuclei was analyzed using confocal fluorescence laser scanning microscopy and a serial *z*-slicing of 0.37 μm optical sections. A surface view (D) and one midsection (E) of a representative nucleus are shown. NPCs were labeled with Imp $\beta^{45-462}$-TRITC (i and iii, red). Scale bar: 10 μm. F,G) HSV1-GFPVP26 viral 0.5 M capsids were incubated with *Xenopus* nuclei harboring functional NPCs for 45 min, labeled with a polyclonal rabbit antiserum raised against intact HSV1 capsids (Remus, bleed V) and colloidal gold with a diameter of 12 nm coated with anti-rabbit antibodies. The specimens were analyzed by field emission scanning electron microscopy. F) 3D surface topography of reconstituted nuclei from different views in the in-lens images (i–iii). The same areas were imaged through a backscatter electron detector revealing the positions of gold-conjugated antibodies (Gi–iii; inverted color mode). HSV1 capsids (white arrowheads) are bound to the cytoplasmic face of the NPCs (white arrows). Scale bar: 100 nm.

**Table 2:** Binding of HSV1 capsids to NPCs of *Xenopus* nuclei reconstituted *in vitro*

| | Functional | | Imp $\beta^{45-462}$ | | BAPTA | |
|---|---|---|---|---|---|---|
| HSV1 capsid | No. of experiments | No. of capsids per nucleus | No. of experiments | No. of capsids per nucleus | No. of experiments | No. of capsids per nucleus |
| 0.1 M | 22 | $7.2 \pm 1.3$ | 4 | $4.6 \pm 0.6$ | 2 | $5.5 \pm 1.5$ |
| 0.5 M | 24 | $14.8 \pm 1.6$ | 4 | $4.2 \pm 0.4$ | 2 | $6.5 \pm 0.5$ |
| 1 M | 22 | $7.5 \pm 1.3$ | 3 | $6.3 \pm 3.0$ | 10 | $3.7 \pm 0.6$ |
| Nuclear | 25 | $13.1 \pm 1.7$ | 3 | $6.7 \pm 3.2$ | 11 | $6.7 \pm 2.1$ |

HSV1 capsids were isolated from extracellular virions using TX-100 in the presence of 0.1, 0.5 or 1 M KCl (viral capsids) or from infected nuclei (nuclear capsids) and incubated with functional *Xenopus* nuclei or with nuclei assembled in the presence of Imp $\beta^{45-462}$ or BAPTA. The samples were fixed, and bound capsids were counted. The number of experiments and the number of capsids bound per nucleus with the standard error of the mean have been tabulated for the different conditions.

FESEM imaging demonstrated that capsids bound specifically to the cytoplasmic surface of NPCs. In cells, incoming HSV1 capsids require microtubule motors for their transport toward NPCs, and indeed viral 0.5 M KCl capsids, but not nuclear C capsids, recruit microtubule motors from *Xenopus* egg and pig brain cytosol (19,20). Notably, both 0.5 M KCl and nuclear C capsids were shown here to bind specifically to NPCs.

*Xenopus* reconstitution reactions can be fine-tuned to block nuclear assembly at specific stages (64,65). The addition of Imp $\beta^{45-462}$ or BAPTA results in the formation of membrane-sealed assembly intermediates that lack any architectural signs of NPCs and are thus considered to be pore-free (49). We observed a residual affinity of HSV1 capsids to such nuclei, which most likely indicates the level of background binding to nuclear envelopes. The preferential binding of 0.5 M KCl and nuclear C capsids cannot be solely attributed to the fact that nuclei assembled in the presence of Imp $\beta^{45-462}$ or BAPTA do not expand as much as in the controls [Figure 4; (49,54)]. While they present a reduced surface area, there was little specificity among the four capsid types in binding to Imp $\beta^{45-462}$ or BAPTA nuclei. By contrast, 0.5 M KCl and nuclear capsids had a significantly higher affinity for nuclei harboring functional NPCs.

### Surface features on HSV1 capsids

Using electron cryo tomography, we have identified substantial differences on the surface of the different capsid types. There were pronounced extra densities on 0.5 M KCl capsids and even more prominent densities on 0.1 M capsids when compared with nuclear C capsids. The shape of these densities is similar to those on cytosolic capsids imaged *in vivo* in the axons of neurons (66), and on viral capsids extracted with detergent and 0.5 M NaCl (67). Previous protein analyses have also revealed differences: whereas nuclear capsids lack tegument proteins, viral 0.5 M KCl capsids contain mainly inner tegument proteins, and viral 0.1 M KCl capsids maintain both inner and outer tegument proteins [summarized in Table 1; (19,20)]. Similar to viral 0.5 M KCl capsids, viral 0.5 M NaCl capsids also contain pUL36 and pUL37 and only low amounts of outer tegument proteins (68).

These data are consistent with the notion that viral capsids extracted with TX-100 and 0.5 M salt maintain additional proteins around their pentons, which most likely include inner tegument proteins. By contrast, we detected only minor structural differences between 1 M KCl viral and nuclear capsids, although the former contain more tegument proteins than the latter [cf. Figure 2; (19,20)]. Apparently these proteins do not form an ordered density on the capsid surface and were therefore not revealed in the icosahedrally symmetrized averages.

### HSV1 proteins interacting with Nups

The outer capsid protein pUL25 and the inner tegument protein pUL36 are likely candidates to target incoming capsids to NPCs.

pUL17 and pUL25 form complexes that connect the pentons and possibly also the portal with the surrounding hexons (69,70). Furthermore, capsid-associated pUL25 is required for proper genome uncoating at the NPC, and biochemical assays have shown that pUL25 can interact with Nup214 and hCG1, two Nups facing the cytosol

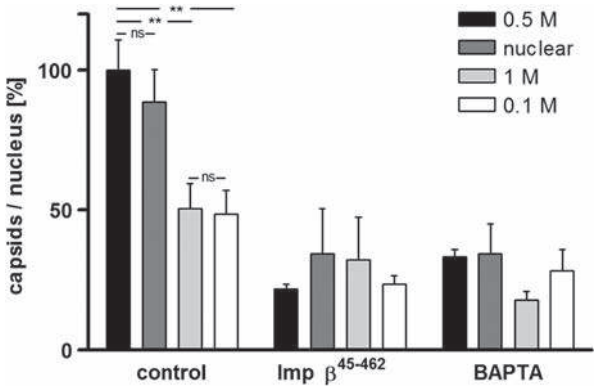


**Figure 5: HSV1 capsid binding to nuclei requires specific capsid surface features and NPCs**. Viral capsids isolated from viral particles with TX-100 and 0.1, 0.5 or 1.0 M KCl or nuclear C capsids were incubated with *Xenopus* nuclei reconstituted *in vitro*. The number of HSV1 capsids bound to nuclei harboring functional NPCs (control) or to nuclei assembled in the presence of Imp $\beta^{45-462}$ or BAPTA was determined by epi-fluorescence microscopy. Images were acquired at different focal planes, merged, bound capsids were counted, and the data were normalized to 100% for 0.5 M viral capsids binding to functional nuclei. The error bars indicate the standard error of the mean. Asterisks indicate $p < 0.0015$ and 'ns' $p > 0.05$ as determined in two-tailed Student's *t*-test.

(39,71–73). pUL25 epitopes are accessible on the surface of the four capsid types tested here, as shown by immunoelectron microscopy of isolated capsids [cf. Table 1; (19)].

pUL36 and pUL37 form complexes that are presumably located at the pentons, and that remain capsid-associated during transport to the nucleus (25,26,28,67,68,71). Antibodies directed against pUL36 reduce nuclear targeting, incoming capsids lacking pUL36 or lacking the N-terminal nuclear localization sequence in pUL36 are not targeted to NPCs, capsids with a point mutation in pUL36 fail to release their genomes, and proteolysis of pUL36 seems to be a prerequisite for the nuclear import of viral DNA (34,74–77). Polyclonal antibodies have access to more pUL36 epitopes on the surface of 0.5 M KCl capsids than on 1 or 0.1 M capsids, whereas pUL36 cannot be detected on nuclear capsids by these antibodies or by mass spectrometry [cf. Table 1; (19)].

Thus, surface-exposed pUL25 could mediate the interaction of both viral 0.5 M KCl and nuclear capsids with NPCs, while surface-exposed pUL36 could only be involved in the association of viral 0.5 M KCl capsids with NPCs. However, additional pUL36 on the 0.5 M KCl capsids when compared with nuclear capsids did not stimulate NPC association. Furthermore, the treatment with 0.1 or 1 M KCl apparently impaired HSV1 factors contributing to NPC binding. The treatment with 1 M salt might perturb the conformation of pUL36, pUL25 or another viral cofactor, while the treatment with 0.1 M KCl might prevent the removal of a putative inhibitor involved in NPC binding. Thus, we were able to demonstrate that the surface of the four HSV1 capsid types harbor structural differences that modulate their capability to interact with *Xenopus* NPCs as well as their affinity to antibodies directed against structural HSV1 proteins. However, so far the molecular and structural details of these changes remain elusive, and could not yet be used to unequivocally pinpoint to specific proteins mediating the interaction of HSV1 capsids with NPCs.

Clearly, more studies are required to characterize the interactions of viral capsids with NPCs. With this new approach, protein domains and peptide motifs suggested by protein–protein interaction assays using isolated proteins could be tested in the context of the complex capsid and NPC structures. Furthermore, this cell-free system may be used to determine the requirements for genome release from the capsids and their import into the nucleoplasm. It provides many advantages: nuclei harboring NPCs but lacking a particular Nup can be generated (62,63), and even for mutants that do not form virions, cell entry can be bypassed if sufficient amounts of viral particles can be generated in heterologous systems. Further insight into capsid docking and viral genome uncoating may be obtained by modulating other host factors such as kinases and by using nuclei lacking specific Nups or capsids harboring subtle mutations. Such studies can identify molecular interactions essential for nuclear targeting, which should be maintained in viral vectors but could be targeted in antiviral therapy.

## Materials and Methods

### HSV1 virion preparation

Extracellular virions of HSV1 strain F (ATCC VR-733) or HSV1-GFPVP26 strain KOS [K26GFP; (56)] were prepared as before (19,33,57). BHK cells (ATCC CCL-10) grown to a density of 1 to

$2 \times 10^7$ cells/175 $cm^2$ flask in MEM (Cytogen) containing 10% fetal calf serum (PAA) were infected with an MOI (multiplicity of infection) of 0.01–0.02 pfu/cell for 2–3 days. The media containing extracellular virions and infected cells were centrifuged at 3000 × ***g*** for 10 min at 4°C. The cell pellet was suspended in an equal volume of TNE (0.5 M NaCl, 20 mM Tris–HCl, pH 7.5, 1 mM ethylenediaminetetraacetic acid, EDTA) to prepare TNE-nuclear capsids, or of MKT (0.1 M KCl, 30 mM MES, 20 mM Tris, pH 7.4) to prepare MKT-nuclear capsids. The cells were aliquoted, frozen in liquid $N_2$ and stored at −80°C. Extracellular viral particles were sedimented from the supernatant at 13,500 × ***g*** for 90 min (Type19 rotor, Beckman Coulter), and the pellet was suspended in MKT buffer, aliquoted, frozen in liquid $N_2$ and stored at −80°C.

## HSV1 capsid preparation

Nuclear capsids were isolated from infected cells that were homogenized in $H_2O$ with 10 mM DTT and protease inhibitors [PI; 10 μg/mL antipain, 2 μg/mL bestatin, 2 μg/mL pepstatin, 2 μg/mL aprotinin, 10 μg/mL E-64, 2 μg/mL leupeptin, 160 μg/mL phenylmethylsulphonyl fluoride (PMSF); Sigma-Aldrich], and the nuclei were sedimented at 230 × ***g*** and 4°C for 7 min and lysed in 1% TX-100 in TNE supplemented with 10 mM DTT and PIs. The capsids were precleared by sedimentation through a 35% sucrose cushion in TNE (with 10 mM DTT and PIs) at 50,000 × ***g*** and 4°C, and then treated with DNAse/RNase for 15 min at 37°C. The capsids were then layered onto linear sucrose gradients (20–50% sucrose in TNE), and banded at 67 000 × ***g*** for 80 min at 4°C (cf. Figure 1, top left; [19, 20, 51, 53)]. The fractions containing the A, B or C capsids were diluted from 1 to 4 with TNE buffer with DTT and PIs, and sedimented at 110,000 × ***g*** (TLA 100.2 rotor, Beckman) for 20 min at 4°C.

Viral capsids were prepared as described before (19,20,37,51). To isolated viral capsids, we mixed the sediment of the medium of infected cells with an equal volume of a twofold capsid lysis buffer [2% (w/v) TX-100 in 0.2, 1 or 2 M KCl, respectively, 20 mM MES, 30 mM Tris, pH 7.4, 20 mM DTT, PIs], incubated for 30 min on ice, and layered onto sucrose cushions [20% (w/v) sucrose in 0.1, 0.5 or 1 M KCl, respectively, 20 mM MES, 30 mM Tris, pH 7.4, 10 mM DTT, PIs]. The capsids were separated from solubilized envelope and tegument proteins by ultracentrifugation at 110 000 × ***g*** for 15 min at 4°C (TLA 100.2 rotor), suspended in BRB80 (80 mM PIPES, pH 6.8, 12 mM $MgCl_2$, 1 mM EGTA, 10 mM DTT, PIs) and treated with 0.1–0.2 U/μL DNAse I (Promega or Roche) and 100 μg/mL RNAse (Roth GmbH) for 30 min at 37°C to facilitate suspension. After an overnight incubation at 4°C, the capsids were sedimented at 110 000 × ***g*** for 15 min at 4°C (TLA 100.2 rotor) and suspended in ELB-S buffer (250 mM sucrose, 50 mM KCl, 10 mM HEPES, pH 7.6, 10 mM DTT, 2.5 mM $MgCl_2$, 1 mg/mL BSA, PIs) using a tip sonifier (Sonic B-12; Branson) at 40 W for initially 3 and up to 10 pulses of 1–2 seconds. If the capsids still appeared clumped by fluorescence microscopy (BX61TRF, 20× objective, Olympus), further pulses were applied. The extent of sonication required for dispersion increased from C capsids to viral capsids isolated at 1, 0.5 or 0.1 M KCl.

## Antibodies

VP5 was detected by mouse monoclonal antibodies (mAb) H1.4 (Biodesign International – Meridian Life Science), VP19c by rabbit polyclonal antibodies (pAb) NC2 (78,79), VP21/22a by pAb NC3/4 (78), VP23 by pAb NC5 (78), pUL25 by mAb #166 (80), pUL36 by pAb #147 (25), pUL37 by pAb pUL37 (26,81) and VP13/14 by pAb R220 (82). NPCs were visualized with fluorescently labeled mAb 414 [A488-120L; Covance; (55)], and DNA with Hoechst 33258 (2 μg/mL; Sigma-Aldrich). HSV1 structural proteins were detected by pAb Remus that has been raised against tegumented capsids (37).

## Immunoblot analysis

Nuclear or viral capsids suspended in sample buffer [1% (w/v) SDS, 50 mM Tris–HCl, pH 6.8, 5% (v/v) glycerol, 1% (v/v) β-mercaptoethanol, 0.001% (w/v) bromphenol blue] were loaded onto 6–16% linear gradient SDS–PAGE gels, and the proteins were transferred to nitrocellulose membranes (Pall Corporation). After blocking with 5% (w/v) fat-free milk in PBS-T [0.1% (v/v) Tween-20, 2.7 mM KCl, 137.9 mM NaCl, 1.5 mM $KH_2PO_4$, 8.1 mM $Na_2HPO_4$, pH 7.4], the membranes were probed with primary antibodies and IRDye anti-rabbit or anti-mouse antibodies (LI-COR Biosciences), and imaged using an Odyssey® Infrared Scanner (LI-COR Biosciences).

## Electron cryo tomography

Viral capsids were sonicated three times for 10 seconds (BB6 cup horn, Sonoplus HD3200, 60% maximal output, Bandelin) directly before adding them onto the grids, and processed for electron cryo tomography as described before (66). Five microliters of a capsid preparation were added together with 2 μL of a homemade colloidal gold suspension (10 nm gold coated with BSA in PBS) onto the holey carbon support film of electron microscopy grids (R2-1, Cu 200 mesh, Quantifoil), and excess liquid was removed by blotting with filter paper. Specimens were vitrified by plunge-freezing into liquid ethane and stored in liquid $N_2$.

Data were collected using transmission electron microscopy; some of the 1 M KCl viral capsid tilt series were collected with a CM300 (43 of the 183 sub-volumes; FEI-Philips), while the rest including the tilt series from other capsid types were collected with a Tecnai Polara (FEI). The microscopes were operated at 300 kV; the pixel size was 0.68 nm (CM300) or 0.81 nm (Polara) at the specimen level, and tilt series were collected with an angular increment of 2° or 3° from −60° to 60°. Defocus was measured along the tilt axis after each tilt and automatically maintained at −8 μm ± 0.5 μm to gain phase contrast. The total electron dose received at the specimen level was kept between 60 and 90 electrons/$Å^2$. The applied electron dose was kept proportional to 1/cos α of the tilt angle (α). Images were acquired on a 2K × 2K Multiscan CCD camera (GIF 2002 post-column energy filter, Gatan).

## Image processing and averaging of tomographic sub-volumes

Alignment of tilted projection image series was performed using 10 nm gold beads as fiducial markers. Three-dimensional reconstructions were calculated using the software IMOD (83), and subsequent processing using Bsoft as described before (66,84). Capsids were located in unbinned tomograms, and sub-volumes with a size of 180 × 180 × 180 pixels were

extracted. The 3D orientation of all sub-volumes was determined using a 22-Å resolution structure of the HSV1 capsid (85) as a template. The oriented sub-volumes were averaged and icosahedral symmetry was applied. Symmetrized averages were used as templates for the next iteration of orientation refinement. Three iterations were performed.

The resolution of the averages was determined by Fourier shell correlation using the 0.5 criterion, after splitting the data into two halves, calculating two separate averages and imposing icosahedral symmetry. To calculate the difference map of the two averages, gray values were scaled to the same radial density maximum within the capsid and minimum just outside of the capsid. The difference in densities was then calculated by subtracting the capsids without tegument from the capsids with tegument. All capsid reconstructions were first scaled against the nuclear C capsid reconstruction. Magnification differences up to 3.5% were detected, and these were compensated for by creating up-scaled or down-scaled maps.

### Reconstitution of nuclei

*Xenopus laevis* egg extracts, cytosolic and membrane fractions, de-membranated sperm chromatin and an ATP regeneration system were prepared, and nuclei were reconstituted within 50–60 min at room temperature (47,64). To assemble pore-free nuclei, 8 μM of recombinant Imp $\beta^{45-462}$ or 5 mM BAPTA (Calbiochem) were added to the mixture and incubated for 60 min (48). In each experiment, the functionality of the reconstituted nuclei was tested by removing a fraction of the nuclei for staining with mAb 414 and Hoechst 33258, and nuclear import analysis with bovine serum albumin coupled to a nuclear localization sequence and to tetramethyl-rhodaminyl-isothiocyanate [TRITC-NLS-BSA; (48,50)].

### Binding of HSV1 capsids to *Xenopus* nuclei

The reconstitution reactions were diluted threefold with 1× ELB-S buffer (pH 7.6, supplemented with 2.5 mM $MgCl_2$), 10 μL of nuclear or viral HSV1 capsids were added to 10 μL of the nuclei and the reactions were agitated at 7 rpm for 20–90 min at room temperature (Figure 1, bottom). Small aliquots were stained with Hoechst 33258 in 12% (w/v) paraformaldehyde, 250 mM sucrose, 10 mM HEPES, pH 7.5, and 0.4% (w/v) *N*-propylgalate for 5 min. Capsid binding to nuclei was analyzed by epi-fluorescence microscopy (UPlanSApo 100× NA 1.4 oil immersion, Olympus BX61TRF equipped with a DP70 digital camera), or by laser scanning confocal fluorescence microscopy (63× NA 1.4 oil immersion, ZEISS LSM 510 META). Ten to twenty-five nuclei of each experimental condition were randomly chosen, and the number of capsids bound to each nucleus was quantified over all focal planes.

### Field emission scanning electron microscopy

*In vitro* reconstituted intact *Xenopus* nuclei incubated with HSV1 capsids for 60 min were labeled with Remus serum. Its dilution was optimized by fluorescence microscopy and adjusted for immunogold labeling. Colloidal gold of 12 nm diameter and coated with goat-anti-rabbit antibodies (Jackson Immuno-Research) was titrated to obtain a minimal background signal in the absence of primary antibodies (64,65). To facilitate the capture of nuclei, they were sedimented at 1000 × ***g*** for 10 min onto silicon chips (Ted Pella) that had been coated with 0.2 mg/mL poly-lysine for 15 min. The chips were transferred to 24-well plates, washed in 1× ELB-K (100 mM KCl, 10 mM HEPES, pH 7.6, 2.5 mM $MgCl_2$, 1 mM DTT, 5 μg/mL cyclohexamide, 5 μg/mL cytochalasin B, 10 μg/mL aprotinin, 10 μg/mL leupeptin), and fixed in 3.7% paraformaldehyde with 0.2% glutaraldehyde (Electron Microscopy Sciences) in 150 mM sucrose, 80 mM PIPES, pH 6.8, 1 mM $MgCl_2$ for 30 min at room temperature. All subsequent steps were as described in 86, with post-fixation in aqueous 0.5% osmium tetroxide, critical-point drying on a CPD030 apparatus (Bal-Tec AG) and sputter coating with 2 nm of chromium (K575X coater, Emitech). The samples were imaged using a FESEM (Ultra plus, ZEISS) with an in-lens detector for secondary electrons to reveal surface structures, and an energy selective backscatter electron detector to localize gold particles.

## Acknowledgments

We thank Katinka Döhner and Anna Buch (Virology, Hannover Medical School) for constructive discussions throughout the study. We are grateful to Prashant Desai for providing HSV1(KOS)-GFPVP26 (Johns Hopkins University, Baltimore, MD) and to Ari Helenius (ETH, Zürich, Switzerland), David M. Meredith (University of Leeds, UK), Gary H. Cohen and Roselyn J. Eisenberg (University of Pennsylvania, PA), Thomas C. Mettenleiter (Friedrich-Loeffler-Institut, Greifswald, Germany) and Valerie G. Preston (University of Glasgow, UK) for generously donating essential antibodies. This study was supported by funds from the *Niedersächsisches Ministerium für Wissenschaft und Kultur* and the *Technion Society* to A. H. and B. S., by the German Research Council (DFG, SFB 900, TP2 to B. S.) and by the *EraNet NanoSci*$^{+}$ *Initiative* to A. H. (ISF 2045/09), B. S. (DFG, So403/4) and K. G. (DFG GR1990/3).

## References

1. Brohawn SG, Partridge JR, Whittle JR, Schwartz TU. The nuclear pore complex has entered the atomic age. Structure 2009;17:1156–1168.
2. Cronshaw JM, Krutchinsky AN, Zhang W, Chait BT, Matunis MJ. Proteomic analysis of the mammalian nuclear pore complex. J Cell Biol 2002;158:915–927.
3. Hetzer MW, Wente SR. Border control at the nucleus: biogenesis and organization of the nuclear membrane and pore complexes. Dev Cell 2009;17:606–616.
4. Frenkiel-Krispin D, Maco B, Aebi U, Medalia O. Structural analysis of a metazoan nuclear pore complex reveals a fused concentric ring architecture. J Mol Biol 2010;395:578–586.
5. Maimon T, Elad N, Dahan I, Medalia O. The human nuclear pore complex as revealed by cryo-electron tomography. Structure 2012;20:998–1006.
6. Cook A, Bono F, Jinek M, Conti E. Structural biology of nucleocytoplasmic transport. Annu Rev Biochem 2007;76:647–671.
7. Pante N, Kann M. Nuclear pore complex is able to transport macromolecules with diameters of about 39 nm. Mol Biol Cell 2002;13:425–434.
8. Wente SR, Rout MP. The nuclear pore complex and nuclear transport. Cold Spring Harb Perspect Biol 2010;2:a000562.

9. Strom AC, Weis K. Importin-beta-like nuclear transport receptors. Genome Biol 2001;2:3008.
10. Fried H, Kutay U. Nucleocytoplasmic transport: taking an inventory. Cell Mol Life Sci 2003;60:1659–1688.
11. Görlich D, Pante N, Kutay U, Aebi U, Bischoff FR. Identification of different roles for RanGDP and RanGTP in nuclear protein import. EMBO J 1996;15:5584–5594.
12. Lee SJ, Matsuura Y, Liu SM, Stewart M. Structural basis for nuclear import complex dissociation by RanGTP. Nature 2005;435:693–696.
13. Davison AJ, Eberle R, Ehlers B, Hayward GS, McGeoch DJ, Minson AC, Pellett PE, Roizman B, Studdert MJ, Thiry E. The order Herpesvirales. Arch Virol 2009;154:171–177.
14. Brown JC, Newcomb WW. Herpesvirus capsid assembly: insights from structural analysis. Curr Opin Virol 2011;1:142–149.
15. Rochat RH, Liu X, Murata K, Nagayama K, Rixon FJ, Chiu W. Seeing the portal in herpes simplex virus type 1 B capsids. J Virol 2011;85:1871–1874.
16. Grünewald K, Desai P, Winkler DC, Heymann JB, Belnap DM, Baumeister W, Steven AC. Three-dimensional structure of herpes simplex virus from cryo-electron tomography. Science 2003;302:1396–1398.
17. Loret S, Guay G, Lippe R. Comprehensive characterization of extracellular herpes simplex virus type 1 virions. J Virol 2008;82:8605–8618.
18. Zhou ZH, Chen DH, Jakana J, Rixon FJ, Chiu W. Visualization of tegument-capsid interactions and DNA in intact herpes simplex virus type 1 virions. J Virol 1999;73:3210–3218.
19. Radtke K, Kieneke D, Wolfstein A, Michael K, Steffen W, Scholz T, Karger A, Sodeik B. Plus- and minus-end directed microtubule motors bind simultaneously to herpes simplex virus capsids using different inner tegument structures. PLoS Pathog 2010;6:e1000991.
20. Wolfstein A, Nagel CH, Radtke K, Dohner K, Allan VJ, Sodeik B. The inner tegument promotes herpes simplex virus capsid motility along microtubules in vitro. Traffic 2006;7:227–237.
21. Kelly BJ, Fraefel C, Cunningham AL, Diefenbach RJ. Functional roles of the tegument proteins of herpes simplex virus type 1. Virus Res 2009;145:173–186.
22. Mettenleiter TC, Klupp BG, Granzow H. Herpesvirus assembly: an update. Virus Res 2009;143:222–234.
23. Johnson DC, Baines JD. Herpesviruses remodel host membranes for virus egress. Nat Rev Microbiol 2011;9:382–394.
24. Henaff D, Radtke K, Lippe R. Herpesviruses exploit several host compartments for envelopment. Traffic 2012;13:1443–1449.
25. Schipke J, Pohlmann A, Diestel R, Binz A, Rudolph K, Nagel CH, Bauerfeind R, Sodeik B. The C terminus of the large tegument protein pUL36 contains multiple capsid binding sites that function differently during assembly and cell entry of herpes simplex virus. J Virol 2012;86:3682–3700.
26. Sandbaumhüter M, Dohner K, Schipke J, Binz A, Pohlmann A, Sodeik B, Bauerfeind R. Cytosolic herpes simplex virus capsids not only require binding inner tegument protein pUL36 but also pUL37 for active transport prior to secondary envelopment. Cell Microbiol 2013;15:248–269.
27. Antinone SE, Smith GA. Retrograde axon transport of herpes simplex virus and pseudorabies virus: a live-cell comparative analysis. J Virol 2010;84:1504–1512.
28. Coller KE, Lee JI, Ueda A, Smith GA. The capsid and tegument of the alphaherpesviruses are linked by an interaction between the UL25 and VP1/2 proteins. J Virol 2007;81:11790–11797.
29. Granzow H, Klupp BG, Mettenleiter TC. Entry of pseudorabies virus: an immunogold-labeling study. J Virol 2005;79:3200–3205.
30. Luxton GW, Haverlock S, Coller KE, Antinone SE, Pincetic A, Smith GA. Targeting of herpesvirus capsid transport in axons is coupled to association with specific sets of tegument proteins. Proc Natl Acad Sci USA 2005;102:5832–5837.
31. Maurer UE, Sodeik B, Grunewald K. Native 3D intermediates of membrane fusion in herpes simplex virus 1 entry. Proc Natl Acad Sci USA 2008;105:10559–10564.
32. Döhner K, Wolfstein A, Prank U, Echeverri C, Dujardin D, Vallee R, Sodeik B. Function of dynein and dynactin in herpes simplex virus capsid transport. Mol Biol Cell 2002;13:2795–2809.
33. Sodeik B, Ebersold MW, Helenius A. Microtubule-mediated transport of incoming herpes simplex virus 1 capsids to the nucleus. J Cell Biol 1997;136:1007–1021.
34. Batterson W, Furlong D, Roizman B. Molecular genetics of herpes simplex virus. VIII. further characterization of a temperature-sensitive mutant defective in release of viral DNA and in other stages of the viral reproductive cycle. J Virol 1983;45:397–407.
35. Granzow H, Weiland F, Jons A, Klupp BG, Karger A, Mettenleiter TC. Ultrastructural analysis of the replication cycle of pseudorabies virus in cell culture: a reassessment. J Virol 1997;71:2072–2082.
36. Miyamoto K, Morgan C. Structure and development of viruses as observed in the electron microscope. XI. Entry and uncoating of herpes simplex virus. J Virol 1971;8:910–918.
37. Ojala PM, Sodeik B, Ebersold MW, Kutay U, Helenius A. Herpes simplex virus type 1 entry into host cells: reconstitution of capsid binding and uncoating at the nuclear pore complex in vitro. Mol Cell Biol 2000;20:4922–4931.
38. Peng L, Ryazantsev S, Sun R, Zhou ZH. Three-dimensional visualization of gammaherpesvirus life cycle in host cells by electron tomography. Structure 2010;18:47–58.
39. Rode K, Dohner K, Binz A, Glass M, Strive T, Bauerfeind R, Sodeik B. Uncoupling uncoating of herpes simplex virus genomes from their nuclear import and gene expression. J Virol 2011;85:4271–4283.
40. Newcomb WW, Booy FP, Brown JC. Uncoating the herpes simplex virus genome. J Mol Biol 2007;370:633–642.
41. Labokha AA, Gradmann S, Frey S, Hulsmann BB, Urlaub H, Baldus M, Gorlich D. Systematic analysis of barrier-forming FG hydrogels from Xenopus nuclear pore complexes. EMBO J 2013;32:204–218.
42. Roos WH, Ivanovska IL, Evilevitch A, Wuite GJ. Viral capsids: mechanical characteristics, genome packaging and delivery mechanisms. Cell Mol Life Sci 2007;64:1484–1497.
43. Yang K, Homa F, Baines JD. Putative terminase subunits of herpes simplex virus 1 form a complex in the cytoplasm and interact with portal protein in the nucleus. J Virol 2007;81:6419–6433.

44. Roos WH, Radtke K, Kniesmeijer E, Geertsema H, Sodeik B, Wuite GJ. Scaffold expulsion and genome packaging trigger stabilization of herpes simplex virus capsids. Proc Natl Acad Sci USA 2009;106:9673–9678.
45. Newmeyer DD, Forbes DJ. Nuclear import can be separated into distinct steps in vitro: nuclear pore binding and translocation. Cell 1988;52:641–653.
46. Newport J. Nuclear reconstitution in vitro: stages of assembly around protein-free DNA. Cell 1987;48:205–217.
47. Harel A, Orjalo AV, Vincent T, Lachish-Zalait A, Vasu S, Shah S, Zimmerman E, Elbaum M, Forbes DJ. Removal of a single pore subcomplex results in vertebrate nuclei devoid of nuclear pores. Mol Cell 2003;11:853–864.
48. Savulescu AF, Shorer H, Kleifeld O, Cohen I, Gruber R, Glickman MH, Harel A. Nuclear import of an intact preassembled proteasome particle. Mol Biol Cell 2011;22:880–891.
49. Macaulay C, Forbes DJ. Assembly of the nuclear pore: biochemically distinct steps revealed with NEM, GTP gamma S, and BAPTA. J Cell Biol 1996;132:5–20.
50. Chan RC, Forbes DI. In vitro study of nuclear assembly and nuclear import using Xenopus egg extracts. Methods Mol Biol 2006;322:289–300.
51. Radtke K, Anderson F, Sodeik B. A precipitation-based assay to analyze interactions of viral particles with cytosolic host factors. Methods Mol Biol 2014;1144:191–208.
52. Newcomb WW, Brown JC. Time-dependent transformation of the herpesvirus tegument. J Virol 2009;83:8082–8089.
53. Newcomb WW, Brown JC. Structure and capsid association of the herpesvirus large tegument protein UL36. J Virol 2010;84:9408–9414.
54. Harel A, Chan RC, Lachish-Zalait A, Zimmerman E, Elbaum M, Forbes DJ. Importin beta negatively regulates nuclear membrane fusion and nuclear pore complex assembly. Mol Biol Cell 2003;14:4387–4396.
55. Wente SR, Rout MP, Blobel G. A new family of yeast nuclear pore complex proteins. J Cell Biol 1992;119:705–723.
56. Desai P, Person S. Incorporation of the green fluorescent protein into the herpes simplex virus type 1 capsid. J Virol 1998;72:7563–7568.
57. Döhner K, Radtke K, Schmidt S, Sodeik B. Eclipse phase of herpes simplex virus type 1 infection: efficient dynein-mediated capsid transport without the small capsid protein VP26. J Virol 2006;80:8211–8224.
58. Kann M, Sodeik B, Vlachou A, Gerlich WH, Helenius A. Phosphorylation-dependent binding of hepatitis B virus core particles to the nuclear pore complex. J Cell Biol 1999;145:45–55.
59. Cohen S, Pante N. Pushing the envelope: microinjection of Minute virus of mice into Xenopus oocytes causes damage to the nuclear envelope. J Gen Virol 2005;86:3243–3252.
60. Porwal M, Cohen S, Snoussi K, Popa-Wagner R, Anderson F, Dugot-Senant N, Wodrich H, Dinsart C, Kleinschmidt JA, Pante N, Kann M. Parvoviruses cause nuclear envelope breakdown by activating key enzymes of mitosis. PLoS Pathog 2013;9:e1003671.
61. Schmitz A, Schwarz A, Foss M, Zhou L, Rabe B, Hoellenriegel J, Stoeber M, Pante N, Kann M. Nucleoporin 153 arrests the nuclear import of hepatitis B virus capsids in the nuclear basket. PLoS Pathog 2010;6:e1000741.
62. Finlay DR, Forbes DJ. Reconstitution of biochemically altered nuclear pores: transport can be eliminated and restored. Cell 1990;60:17–29.
63. Walther TC, Fornerod M, Pickersgill H, Goldberg M, Allen TD, Mattaj IW. The nucleoporin Nup153 is required for nuclear pore basket formation, nuclear pore complex anchoring and import of a subset of nuclear proteins. EMBO J 2001;20:5703–5714.
64. Rotem A, Gruber R, Shorer H, Shaulov L, Klein E, Harel A. Importin beta regulates the seeding of chromatin with initiation sites for nuclear pore assembly. Mol Biol Cell 2009;20:4031–4042.
65. Shaulov L, Harel A. Improved visualization of vertebrate nuclear pore complexes by field emission scanning electron microscopy. Structure 2012;20:407–413.
66. Ibiricu I, Huiskonen JT, Dohner K, Bradke F, Sodeik B, Grunewald K. Cryo electron tomography of herpes simplex virus during axonal transport and secondary envelopment in primary neurons. PLoS Pathog 2011;7:e1002406.
67. Cardone G, Newcomb WW, Cheng N, Wingfield PT, Trus BL, Brown JC, Steven AC. The UL36 tegument protein of herpes simplex virus 1 has a composite binding site at the capsid vertices. J Virol 2012;86:4058–4064.
68. Newcomb WW, Jones LM, Dee A, Chaudhry F, Brown JC. Role of a reducing environment in disassembly of the herpesvirus tegument. Virology 2012;431:71–79.
69. Cockrell SK, Huffman JB, Toropova K, Conway JF, Homa FL. Residues of the UL25 protein of herpes simplex virus that are required for its stable interaction with capsids. J Virol 2011;85:4875–4887.
70. Conway JF, Cockrell SK, Copeland AM, Newcomb WW, Brown JC, Homa FL. Labeling and localization of the herpes simplex virus capsid protein UL25 and its interaction with the two triplexes closest to the penton. J Mol Biol 2010;397:575–586.
71. Pasdeloup D, Blondel D, Isidro AL, Rixon FJ. Herpesvirus capsid association with the nuclear pore complex and viral DNA release involve the nucleoporin CAN/Nup214 and the capsid protein pUL25. J Virol 2009;83:6610–6623.
72. Preston VG, Murray J, Preston CM, McDougall IM, Stow ND. The UL25 gene product of herpes simplex virus type 1 is involved in uncoating of the viral genome. J Virol 2008;82:6654–6666.
73. Trus BL, Newcomb WW, Cheng N, Cardone G, Marekov L, Homa FL, Brown JC, Steven AC. Allosteric signaling and a nuclear exit strategy: binding of UL25/UL17 heterodimers to DNA-Filled HSV-1 capsids. Mol Cell 2007;26:479–489.
74. Abaitua F, Hollinshead M, Bolstad M, Crump CM, O'Hare P. A Nuclear localization signal in herpesvirus protein VP1-2 is essential for infection via capsid routing to the nuclear pore. J Virol 2012;86:8998–9014.
75. Copeland AM, Newcomb WW, Brown JC. Herpes simplex virus replication: roles of viral proteins and nucleoporins in capsid-nucleus attachment. J Virol 2009;83:1660–1668.
76. Jovasevic V, Liang L, Roizman B. Proteolytic cleavage of VP1-2 is required for release of herpes simplex virus 1 DNA into the nucleus. J Virol 2008;82:3311–3319.

77. Roberts AP, Abaitua F, O'Hare P, McNab D, Rixon FJ, Pasdeloup D. Differing roles of inner tegument proteins pUL36 and pUL37 during entry of herpes simplex virus type 1. J Virol 2009;83:105–116.
78. Cohen GH, Ponce de Leon M, Diggelmann H, Lawrence WC, Vernon SK, Eisenberg RJ. Structural analysis of the capsid polypeptides of herpes simplex virus types 1 and 2. J Virol 1980;34:521–531.
79. Eisenberg RJ, Long D, Ponce de Leon M, Matthews JT, Spear PG, Gibson MG, Lasky LA, Berman P, Golub E, Cohen GH. Localization of epitopes of herpes simplex virus type 1 glycoprotein D. J Virol 1985;53:634–644.
80. Thurlow JK, Murphy M, Stow ND, Preston VG. Herpes simplex virus type 1 DNA-packaging protein UL17 is required for efficient binding of UL25 to capsids. J Virol 2006;80:2118–2126.
81. Leege T, Granzow H, Fuchs W, Klupp BG, Mettenleiter TC. Phenotypic similarities and differences between UL37-deleted pseudorabies virus and herpes simplex virus type 1. J Gen Virol 2009;90:1560–1568.
82. Whittaker GR, Riggio MP, Halliburton IW, Killington RA, Allen GP, Meredith DM. Antigenic and protein sequence homology between VP13/14, a herpes simplex virus type 1 tegument protein, and gp10, a glycoprotein of equine herpesvirus 1 and 4. J Virol 1991;65:2320–2326.
83. Kremer JR, Mastronarde DN, McIntosh JR. Computer visualization of three-dimensional image data using IMOD. J Struct Biol 1996;116:71–76.
84. Heymann JB, Belnap DM. Bsoft: image processing and molecular modeling for electron microscopy. J Struct Biol 2007;157: 3–18.
85. Cheng N, Trus BL, Belnap DM, Newcomb WW, Brown JC, Steven AC. Handedness of the herpes simplex virus capsid and procapsid. J Virol 2002;76:7855–7859.
86. Allen TD, Rutherford SA, Murray S, Sanderson HS, Gardiner F, Kiseleva E, Goldberg MW, Drummond SP. Generation of cell-free extracts of Xenopus eggs and demembranated sperm chromatin for the assembly and isolation of in vitro-formed nuclei for Western blotting and scanning electron microscopy (SEM). Nat Protoc 2007;2: 1173–1179.
87. Loret S, Lippe R. Biochemical analysis of infected cell polypeptide (ICP)0, ICP4, UL7 and UL23 incorporated into extracellular herpes simplex virus type 1 virions. J Gen Virol 2012;93:624–634.
88. Roizman B, Campadelli-Fiume G. Alphaherpes viral genes and their functions. In: Arvin A, Campadelli-Fiume G, Mocarski E, Moore PS, Roizman B, Whitley R, Yamanishi K, editors. Human Herpesviruses, Biology, Therapy and Immunoprophylaxis. New York: Cambridge University Press; 2007, pp. 70–92.
89. Toropova K, Huffman JB, Homa FL, Conway JF. The herpes simplex virus 1 UL17 protein is the second constituent of the capsid vertex-specific component required for DNA packaging and retention. J Virol 2011;85:7513–7522.